Hindawi
Journal of Nanotechnology
Volume 2020, Article ID 3683629, 16 pages
https://doi.org/10.1155/2020/3683629

Research Article

Adsorption Capacities of Hygroscopic Materials Based on NaCl-TiO_2 and NaCl-SiO_2 Core/Shell Particles

Marie Bermeo,[1] Nabil El Hadri,[1] Florent Ravaux,[1] Abdelali Zaki,[2] Linda Zou,[2] and Mustapha Jouiad [1,3]

[1]*Department of Mechanical & Materials Science and Engineering, Khalifa University of Science and Technology, Abu Dhabi, UAE*
[2]*Department of Civil Infrastructure and Environmental Engineering, Khalifa University of Science and Technology, Abu Dhabi, UAE*
[3]*Laboratory of Physics of Condensed Mater (LPMC), University of Picardie Jules Verne, Amiens 80039, France*

Correspondence should be addressed to Mustapha Jouiad; mustapha.jouiad@u-picardie.fr

Received 23 September 2019; Accepted 11 December 2019; Published 13 February 2020

Guest Editor: Giorgio Vilardi

Copyright © 2020 Marie Bermeo et al. This is an open access article distributed under the Creative Commons Attribution License, which permits unrestricted use, distribution, and reproduction in any medium, provided the original work is properly cited.

Hygroscopic materials which possess high moisture adsorption capacity were successfully upgraded by the functionalization of sodium chloride (NaCl) using two nuances of oxides. A procedure was developed to first prepare submicron-sized NaCl crystals; thereafter, these crystals were coated by choice of either titanium dioxide (TiO_2) or silica (SiO_2) to enhance the hygroscopic properties of NaCl and prevent its premature deliquescence. After coating, several analytical techniques were employed to evaluate the obtained composite materials. Our findings revealed that both composites NaCl-TiO_2 and NaCl-SiO_2 gave excellent performances by exhibiting interesting hydrophilic properties, compared to the sole NaCl. This was demonstrated by both environmental scanning electron microscope (ESEM) and water vapor adsorption experiments. In particular, NaCl-TiO_2 composite showed the highest water adsorption capacity at low relative humidity and at a faster adsorption rate, induced by the high surface energy owing to the presence of TiO_2. This result was also confirmed by the kinetics of adsorption, which revealed that not only does NaCl-TiO_2 adsorb more water vapor than NaCl-SiO_2 or sole NaCl but also the adsorption occurred at a much higher rate. While at room temperature and high relative humidity, the NaCl-SiO_2 composite showed the best adsorption properties making it ideal to be used as a hygroscopic material, showing maximum adsorption performance compared to NaCl-TiO_2 or sole NaCl. Therefore, NaCl-TiO_2 and NaCl-SiO_2 composites could be considered as promising hygroscopic materials and potential candidates to replace the existing salt seeding agents.

1. Introduction

Hygroscopic materials are characterized for their ability to attract and hold water molecules from their surrounding environment. This property has led to numerous applications such as drying agents for moisture-sensitive products (e.g., electronic devices, food, and pharmaceutical products), dehumidifiers, humectants for cosmetic products, adsorbents for industrial adsorption processes [1–4], and aerosols for rain enhancement and water harvesting [5–9]. Sodium chloride (NaCl) is a well-known hygroscopic material which is commonly used as an adsorbent. It is also used as a cloud seeding agent for warm clouds, i.e., hygroscopic cloud seeding, to enhance precipitation due to its affinity towards water [10–13]. Although NaCl and other natural materials are widely used for their good adsorption properties, it remains a challenge to advance the fabrication of new materials with better performances than conventional ones, in terms of two main criteria, namely, higher water uptake and optimum adsorption kinetics at variable conditions of temperature and relative pressure.

In this regard, several complex hygroscopic materials have been developed based on porous materials such as metal-organic framework. For instance, MOF-801 and MOF-841 achieved water adsorption as high as 380 $cm^3\,g^{-1}$ and 550 $cm^3\,g^{-1}$, respectively, at low relative pressure of 0.3, and this performance was evaluated in the temperature range of 15°C to 55°C [14, 15]. Polyacrylamide (PAM) and

sodium polyacrylate (PAAS) are known as superhygroscopic porous materials. They were found to act as a catalyst powder to enhance precipitations with a lower efficiency for PAAS [16]. While other composite adsorbents such as crystalline MCM-41 and calcium chloride ($CaCl_2$) have revealed a high water adsorption capacity of 1.75 kg kg^{-1} in the temperature range of 10–15°C and at 78–92% relative humidity (RH) [17, 18]. Although these materials have very good hygroscopic properties, several factors such as their complex processing routes and their water stability at different conditions of pressure and temperature limit their use especially in cloud seeding.

For cloud seeding applications, the hygroscopic materials need to meet the particle size requirement criterion. According to earlier studies [19–22] based on numerical correlations, modelling, and simulations, the optimum size of seeding materials is in the range of 0.5 to 10 μm in diameter. This particle size range ensures an efficient collision-coalescence process of the cloud condensation nuclei (CCN). This process initiates the water droplet nucleation and enables their growth until they reach the raindrop critical size of about 24 μm in diameter [23]. At this stage, the raindrops may overcome the updraft velocity inside the clouds and be dragged downwards by their own weight to fall as rain [24, 25].

This study concerns the characterization of novel composite materials which were developed through relatively simple mechanisms and using affordable and abundant materials in nature. Here, commercial salt (NaCl) as a raw material was optimized, in terms of size as per cloud seeding requirement, to yield to NaCl crystals with sub-micrometric size. Thereafter, they were coated with thin layers of oxides, either TiO_2 or SiO_2, which have good affinity towards water, i.e., hydrophilicity [26–29], water adsorption [30, 31], and solubility [32–36]. A characterization of the benchmark NaCl particles was carried out to have a baseline reference to be compared to the NaCl-TiO_2 and NaCl-SiO_2 composites obtained after the coating process.

1.1. Hygroscopicity. A hygroscopic solid material can be identified through its hygroscopic point and water uptake capacity. The hygroscopic point ($h_{g.p.}$) represents the threshold value of the relative humidity in the air above which the solid substance starts adsorbing water vapor [37]. It describes the relationship at equilibrium between the water vapor pressure (P_{sol}) and its surrounding environment with respect to the partial pressure of the water vapor in the air (P_{H2O}) at a specific temperature. $h_{g.p.}$ is generated as a percentage given by

$$h_{g.p.} = \left(\frac{P_{sol}}{P_{H_2O}}\right) \times 100\%. \quad (1)$$

If the solid is a water-soluble material such as soluble salts, then P_{sol} represents the water vapor pressure in the solid saturated solution since it already contains a certain amount of moisture at equilibrium prior to saturation. In this case, at the hygroscopic point, the solid material starts experiencing the deliquescence process while adsorbing water vapor from the atmosphere until it starts dissolving rapidly at quasi-constant RH, generally represented by the quasi-vertical line in the isotherm at high RH. This deliquescence property is a characteristic of certain hygroscopic solid compounds, e.g., water-soluble salts, which experience a phase transition from a solid particle to a liquid drop, i.e., to form a solution [38, 39]. Hence, the hygroscopic point of this type of materials at which the deliquescence process occurs is also called deliquescence point or deliquescence relative humidity (DRH) [40–42].

2. Materials and Methods

2.1. Material Synthesis. The chemical compounds were purchased from Sigma-Aldrich with analytical grade. Three types of samples were prepared: (i) optimized neat NaCl with submicron-range particles, (ii) NaCl coated either with titanium dioxide (NaCl-TiO_2), or (iii) silicon dioxide (NaCl-SiO_2). Here, the optimization of NaCl consists of achieving a particle size reduction of commercial NaCl to match the aforementioned size requirements (0.5 to 10 μm) for seeding materials. Herein, an aqueous solution was prepared using commercial salt, and then 1 ml of this solution was added to 50 ml of 2-propanol while stirring. Once a white precipitate is observed, the NaCl crystals were extracted by either centrifugation or filtration, followed by drying in the oven at 80°C. For the synthesis of NaCl-TiO_2 core-shell composite, similar to what was reported by our previous work [43], first TiO_2 solution was prepared by hydrolysis of titanium (IV) butoxide solution as the first step. Solution A was prepared by dispersing 5 ml titanium (IV) butoxide in 40 ml of 2-propanol. Then, solution B was prepared by mixing 50 ml of deionized water and 1 ml of nitric acid. Subsequently, solution B was added dropwise into solution A under vigorous stirring until the formation of a semitransparent TiO_2 solution. A pH control below 2 is crucial to ensure the overall NaCl-TiO_2 particle size in the submicron range. To prepare NaCl-TiO_2 composite, a solution of 50 mg of optimized NaCl and 10 ml of 2-propanol was needed. Then, 1 ml of the above-prepared TiO_2 solution was poured dropwise into this NaCl solution. The new NaCl-TiO_2 solution was stirred vigorously for 60 minutes to be ready for the separation process by centrifugation, drying at 80°C overnight and calcination at 250°C during 3 hours.

For the synthesis of NaCl-SiO_2 core-shell composite, first SiO_2 solution was prepared by the hydrolysis of the tetraethyl orthosilicate (TEOS) solution. An acid solution was prepared by mixing 1.6 ml of hydrochloric acid with 20 ml of ethanol and 20 ml of deionized water. Then, 4.6 ml of TEOS solution was added dropwise into the acidic solution under vigorous stirring. pH was kept at 2 while stirring at 250 rpm for 2 hours. To prepare NaCl-SiO_2 composite, a solution of 50 mg of optimized NaCl and 2 ml of 2-propanol was needed. Then, 1 ml of the above-prepared SiO_2 solution was poured dropwise into this NaCl solution. The new NaCl-SiO_2 solution was stirred vigorously for 60 minutes to be ready for the separation process by centrifugation, drying at 80°C overnight and calcination at 550°C during 3 hours.

2.2. Characterization. Morphology and the size of the synthesized samples were characterized by scanning electron microscopy (SEM), FEI™ Quanta 250, operating at 5 KV, and their elemental composition analysis was determined using energy dispersive X-ray spectroscopy (EDS) from EDAX™. Additional composition analysis was performed using Fourier-transform infrared spectroscopy (FTIR) using a Bruker™ Optics VERTEX system recorded at a wavenumber range of 4000–400 cm^{-1} and Raman spectroscopy from WiTec™ with a laser source of 532 nm. The thin layers of TiO_2 and SiO_2 coating NaCl crystals were revealed by energy-filtered transmission electron microscopy (EFTEM) using GATAN™ and electron energy loss spectroscopy (EELS), energy filter mounted on Titan FEI™ transmission electron microscope (TEM) operating at 300 KV. TEM samples were prepared by dispersion in isopropanol solvent of a powder made of particles and applied to 3 mm Cu grids coated with carbon film.

In situ water vapor condensation was performed by environmental scanning electron microscopy (ESEM) consisting of SEM operating at variable pressure and a gaseous secondary electron detector (GSED) designed for general wet imaging. The *in situ* water condensation setup is shown in Figure 1(a). The condensation experiments were conducted for each sample separately at 10 KV, at variable pressure and at constant temperature of 1°C. To ensure thermal stability on the surface of the sample, cooling at 1°C for a dwell time of 30 minutes was required [44, 45]; thereafter, vapor pressure inside the chamber was increased gradually until the dew point was reached, i.e., formation of water droplets, as per the path shown in the water phase diagram in Figure 1(b). The experimental setup allowed observation of the water droplet nucleation, formation, and growth. The entire water droplet process was then recorded and analyzed frame by frame. The evaluation of the surface wettability and deliquescence of the samples was carried out by the comparison between the diameter of the dried particles under high vacuum and the wet particles during condensation, along with the examination of the altered solid particles after condensation.

A Quantachrome™ Instruments' VSTAR vapor sorption volumetric analyzer was used to record the water adsorption-desorption isotherms, water adsorption capacity, and kinetics of adsorption. The relative pressure (P/P_0) was varied within a range 0–1 equivalent to 0–99% RH. The isosteric heat of adsorption was deduced for each sample from the adsorption isotherms obtained at temperatures of 25°C, 35°C, and 45°C. TA Instruments™ DMA Q800 Dynamic Mechanical Analysis (DMA) in conjunction with a DMA-RH accessory was used to compare qualitatively the mechanical integrity which represents the water adsorption capacity and the deliquescence of the materials. The samples were prepared by compacting the powder samples into a circular disc shape. Water vapor at controlled RH and at equilibrium state was introduced gradually, while the DMA clamp was maintained at a constant compression load of 0.1 N at a room temperature. The result is given as displacements of the clamp in contact with the sample versus RH. The DMA-RH operates from 5 to 90% RH using Peltier elements allowing a precise temperature and RH control of ±0.1°C and ±3% RH, respectively.

3. Results and Discussion

3.1. Morphology and Chemical Composition. Commercial NaCl exhibits random particle sizes mostly greater than 100 μm (Figure 2(a)). To optimize the particle size and to obtain cubic-shaped NaCl particles, a systematic analysis of the agglomerated particles was performed. As a result, a remarkable particle size reduction and individual cubic-shaped NaCl particles arose as an effect of 2-propanol (Figure 2(b)). The optimized NaCl particles obtained by centrifugation have a size ranging from 1 to 6 μm with an average size of 2.3 ± 0.9 μm in length (Figure 2(c)), whereas the ones obtained by filtration have a significantly reduced size ranging from 0.5 and 1.3 μm, with an average size of 0.8 ± 0.2 μm in length (Figure 2(d)). The resultant particle size distribution of the optimized NaCl then appeared to fall within the aforementioned optimum size range for hygroscopic cloud seeding agents as described in the literature [19–22]. Hence, these optimized NaCl particles were used for the coating process.

After the coating process, the morphology and composition of the NaCl-TiO_2 and NaCl-SiO_2 composites were analyzed. SEM micrographs showed uniform particles, i.e., mostly cubic shape and homogeneous size. NaCl-TiO_2 particle sizes ranging from 0.3 to 1.1 μm with an average size of 0.566 ± 0.152 μm in length are the smallest particles achieved (Figure 3(a)). Similarly, an optimum size for NaCl-SiO_2 was obtained with a particle size range between 0.9–6.9 μm and an average of 2.8 ± 1.2 μm in length (Figure 3(b). Furthermore, both composites, NaCl-TiO_2 and NaCl-SiO_2, showed that, during the coating process, the cubic-shaped particles were not destroyed, and they fulfilled the criterion related to the particle size distribution for seeding agents.

EDS elemental composition analysis for the studied samples is represented in Figure 4. A reference EDS spectrum obtained from the optimized NaCl showed Na and Cl peaks (Figure 4(a)), which indicates no contamination during the optimization process. NaCl-TiO_2 composite showed EDS spectra of high peaks of Na and Cl and very small peaks of Ti and O_2 (Figure 4(b)). Likewise, NaCl-SiO_2 composite showed EDS spectra of high peaks of Na and Cl and small peaks of Si and O_2 (Figure 4(c)). In both cases, the EDS composition quantification results indicate that the approximate weight percentage of the oxides in both composites is below 5%.

FTIR analysis revealed the composition of both composites NaCl-TiO_2 and NaCl-SiO_2 (Figure 5). Sole TiO_2 showed FTIR spectra of high absorbance band in the region 500–1000 cm^{-1}, which is certainly due to the bonds between the titanium and the oxygen Ti-O. This is confirmed by the FTIR spectra of the NaCl-TiO_2 composite where the bond Ti-O is present. However, due to the amount of TiO_2 coating in the composite sample (≤5%), the absorbance band observed is significantly low as expected (Figure 5(a)). Similarly, the FTIR spectra of the NaCl-SiO_2 composite showed the presence of three distinctive peaks of low intensity at

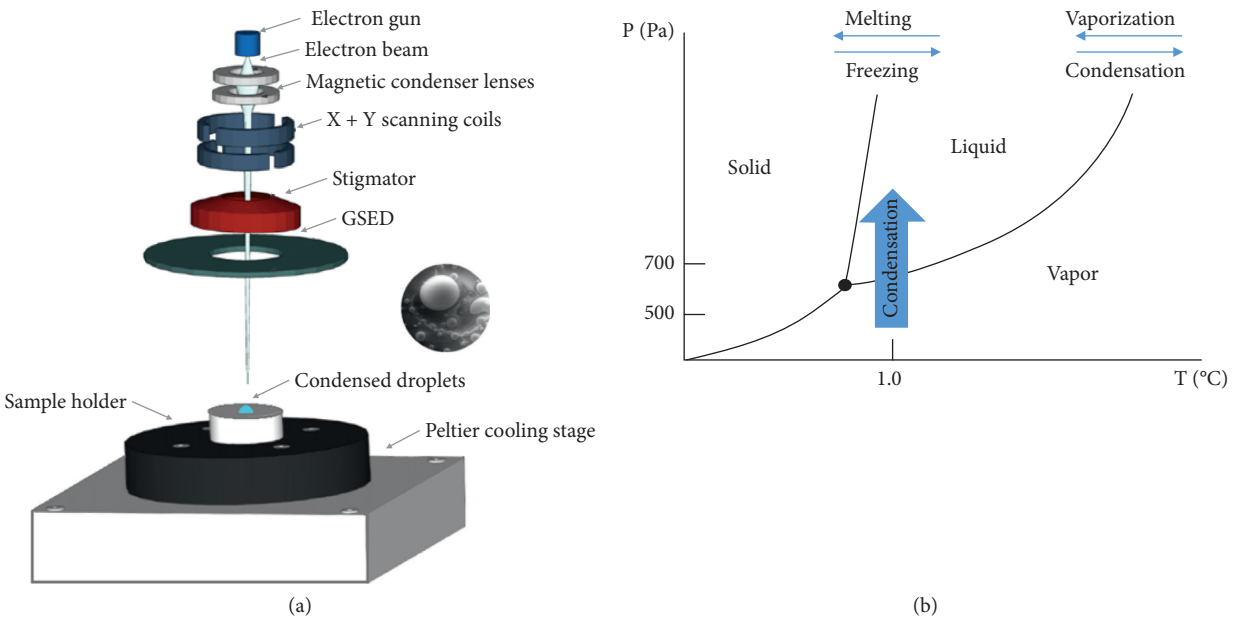

Figure 1: (a) Experimental setup for *in situ* water condensation (ESEM) [42]; (b) water condensation was achieved at a temperature of 1°C and increasing the pressure above 500 Pa.

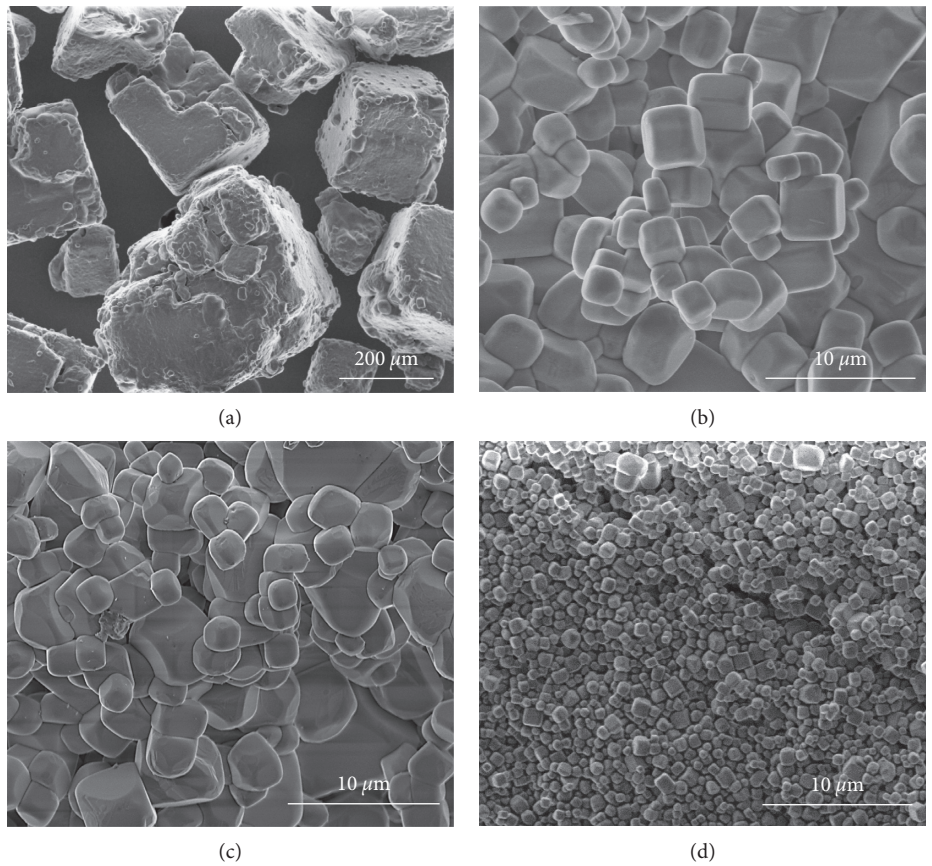

Figure 2: SEM micrographs showing different obtained sizes of NaCl. Sequence 1: (a) commercial NaCl; (b) NaCl after using 2-propanol; and (c) NaCl obtained by centrifugation. Sequence 2: (a) and (b) followed by (d) NaCl obtained after filtration.

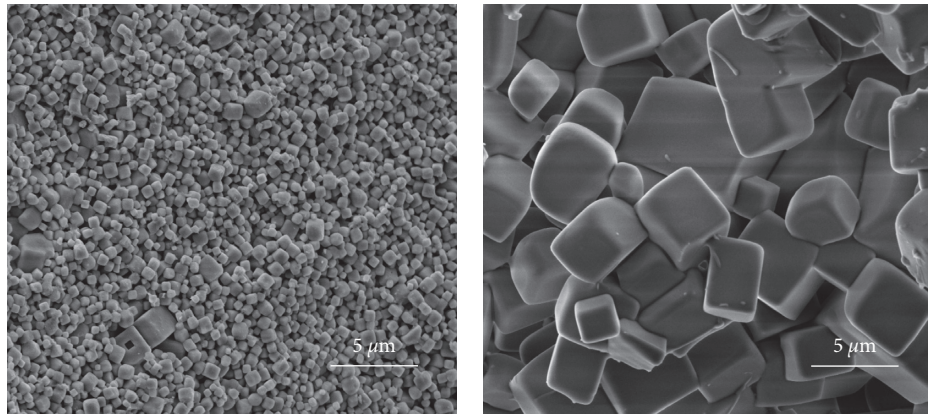

(a) (b)

Figure 3: SEM micrographs of (a) NaCl-TiO_2 and (b) NaCl-SiO_2.

1050 cm^{-1}, 790 cm^{-1}, and 430 cm^{-1} compared to the high absorbance peaks observed for the sole SiO_2 at the same wavenumber (Figure 5(b)).

Additionally, Raman spectroscopy was also used to confirm the characteristic structural fingerprint of the samples NaCl, NaCl-TiO_2, and TiO_2 (Figure 6). As expected, due to the symmetry of NaCl crystals, no Raman signal was detected for NaCl; however, TiO_2 revealed Raman spectra with several peaks in 0–1000 cm^{-1} range and a prominent peak at 152 cm^{-1}. This is a characteristic peak of the anatase phase of TiO_2 [46, 47]. A zoomed-in (inset) figure shows that NaCl-TiO_2 possesses a peak at a Raman shift of 152 cm^{-1}, approximately, which confirms the presence of TiO_2 in the composite material.

Undoubtedly, the oxides TiO_2 and SiO_2 are present in the NaCl-TiO_2 and NaCl-SiO_2 composites, respectively. Hence, in order to verify the quality of TiO_2 and SiO_2 coatings in terms of dispersion and homogeneity, EFTEM and EELS observations were conducted. As a result, an evenly distributed thin layer of TiO_2 on the surface of the NaCl-TiO_2 composite was observed. The TiO_2 coating thickness is approximately 8 nm, which varies slightly from one particle to another (Figure 7).

Likewise, an evenly distributed thin layer of SiO_2 was observed on the surface of the NaCl-SiO_2 composite (Figure 8). The thickness of the coating of SiO_2 surrounding the NaCl particle seems to vary approximately between 8 nm and 12 nm.

For both EFTEM-EELS images, the interaction of the electron beam and the sample creates a shadow effect observed in both images, where the intensity of the thin layer, either Ti or Si, seems to be concentrated in some edges of the particle.

3.2. Water Sorption Analysis. A solid substance is considered as an efficient hygroscopic material when it shows high water adsorption capacity and high rate of adsorption. This is generally the case for porous material possessing high specific surface area or micropore volume, as well as a large pore network [48]. These characteristics can be estimated through the isotherms obtained during the sorption analysis. Besides, the hygroscopic materials being considered as cloud seeding agents are required to exhibit a high-water adsorption capacity especially at low RH and low temperature. Hence, both water adsorption capacity and kinetics of adsorption along with deliquescence are essential parameters to determine the best seeding agent.

In this sense, the hygroscopic properties of the successfully synthesized NaCl-TiO_2 and NaCl-SiO_2 composites compared to neat NaCl were studied to determine their performances under specific conditions. Adsorption isotherms of these materials were obtained at three different temperatures: 25°C, 35°C, and 45°C (Figure 9). The adsorption isotherms exhibited particular performances for all samples in two different stages: at low relative pressure (stage 1), from 0 to 0.6 of relative pressure (i.e., 0 to 60% RH), and at high relative pressure (stage 2), from 0.6 to 1 of relative pressure (i.e., 60 to 99% RH).

At stage 2, multilayer adsorption mechanism and subsequently full deliquescence of the solid adsorbents are reflected on the very steep lines against a very slight increase in relative pressure. The optimized NaCl has comparable water uptakes at all temperatures and a hygroscopic point at approximately 75% RH, which are in accordance with the Extended Aerosol Inorganics Model IV (E-AIM) [49–51] and previous studies [52–56]. The water uptake of neat NaCl above the hygroscopic point at 25°C (3 data points) was correlated to E-AIM as it showed an experimental deviation (Figure 9(a)). Several studies have examined that anatase TiO_2 [27] and amorphous SiO_2 [57–59] exhibit a moderate water uptake as the relative pressure increases. Thus, the steep isotherms of the NaCl-TiO_2 and NaCl-SiO_2 composites at high relative pressure imply that they were boosted by the deliquescence of NaCl (Figures 9(b) and 9(c)).

At stage 1, new graphs were obtained from the full range of relative pressure. These graphs were plotted separately in order to comprehend the adsorption process behavior (Figures 9(d)–9(f)). Here, the temperature seems to be an active kinetics parameter influencing the water uptake at low

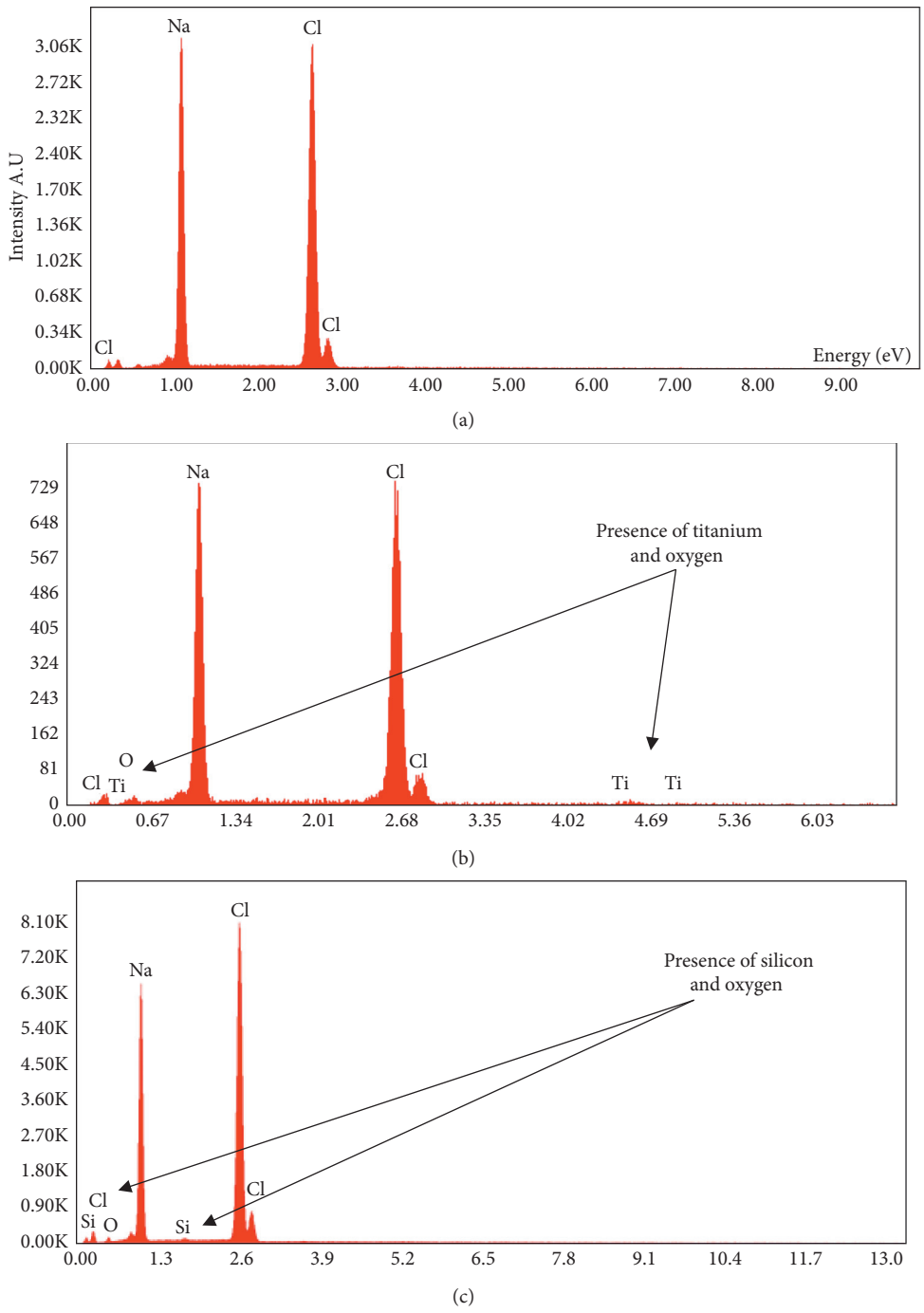

Figure 4: EDS spectra of (a) reduced size NaCl, (b) NaCl-TiO_2, and (c) NaCl-SiO_2.

relatively pressure, even though this stage is related to a monolayer adsorption mechanism. Nevertheless, a similar trend among the samples was observed, i.e., the higher the temperature, the higher the water uptake across the adsorption isotherms. As expected, a slight change in water uptake for NaCl was observed as the relative pressure increases [60–62]. Thus, a nonsignificant influence of NaCl can be inferred on the NaCl-TiO_2 and NaCl-SiO_2 composites at low relative pressure.

The best hygroscopic materials for cloud seeding applications are those capable of adsorbing high amounts of moisture especially at very low relative pressure, i.e., low RH. This is in consideration of the variable pressure profile in the atmosphere and low relative RH, especially in low cloud cover conditions [63, 64]. Accordingly, special attention was given to the analysis of the isotherms at stage 1 (low relative pressure) to evaluate the performances of the samples. Therefore, a comparison of the adsorption isotherms of the

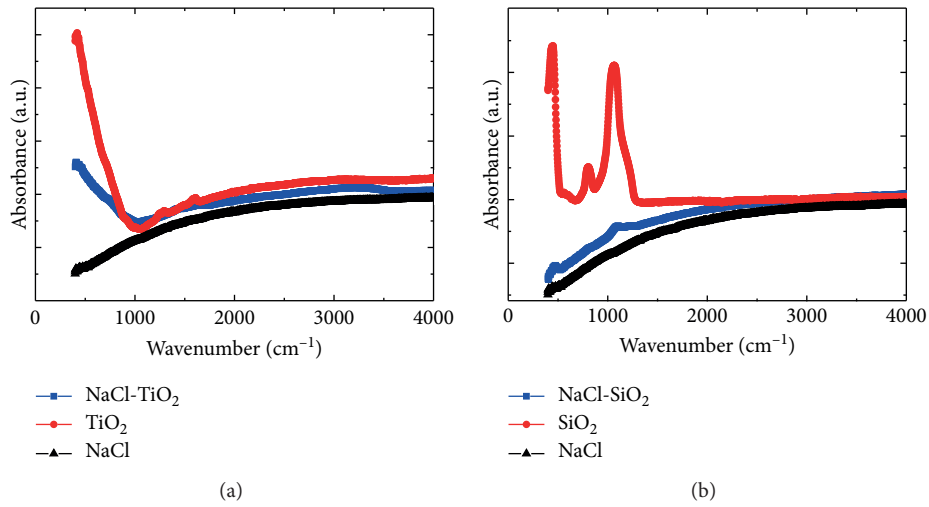

Figure 5: FTIR spectra of (a) NaCl-TiO_2 and (b) NaCl-SiO_2.

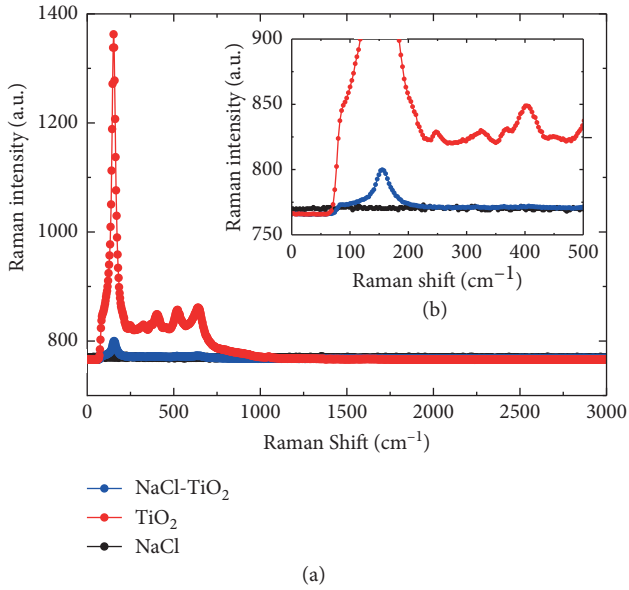

Figure 6: Raman spectra of NaCl, TiO_2, and NaCl-TiO_2. The inert (0 to 500 cm^{-1}) highlights the peak at 152 cm^{-1} approximately, which is the characteristic of TiO_2.

samples were plotted at stage 1 at temperatures of 25°C, 35°C, and 45°C (Figure 10).

According to the IUPAC classification for the adsorption isotherms for gas-solid equilibria [61], at low relative pressure, NaCl-TiO_2 composite followed a sigmoid-shaped isotherm curve, thus reflecting a type IV isotherm. Monolayer-multilayer adsorption attributed to high energy of adsorption is the characteristic of this isotherm [65, 66]. Undoubtedly, NaCl-TiO_2 exhibited the highest water uptake due to the contribution of TiO_2. The surface energy of this oxide facilitates the interaction between the water vapor molecules and the surface of the NaCl-TiO_2. Similarly, NaCl-SiO_2 and NaCl followed the type IV isotherm, but with lower water uptake which indicates less interaction of water molecules with these samples attributed to a minor surface energy of SiO_2 and NaCl, respectively. Overall and for all temperatures, NaCl-TiO_2 shows the highest performance in comparison with NaCl and NaCl-SiO_2. At 25°C, NaCl-TiO_2 showed an increase of water uptake up to 360% with respect to NaCl or NaCl-SiO_2. At 35°C and 45°C, the increase of water uptake reached more than 1000%. Moreover, by increasing the temperature, the water uptake for NaCl-TiO_2 increased from 34.7 mg g^{-1} at 25°C to 140.1 mg g^{-1}at 45°C. These results indicate that TiO_2 significantly enhances the hygroscopicity of the NaCl-TiO_2 composite promoting it as potential candidate for cloud seeding.

At stage 2 (high relative pressure), the effect of the coating on hygroscopicity was not conclusive as it gave mixed results (Figure 11).

It is important to point out that the highest relative pressure at which the maximum water uptake was measured is not accurately 1 (100% RH) for all the samples. The highest relative pressures oscillate in the range of (0.9768–0.9832). As a result, the difference between water uptake at both extreme values of relative pressure may be significant. For example, as per the E-AIM model, NaCl at 25°C (298.15 K) has a water uptake of 24349 mg g^{-1} at 97.68% RH, and 33555 mg g^{-1} at 98.32% RH. Therefore, for close values of water uptake among the samples, the difference may be negligible. At 25°C and 35°C NaCl-SiO_2 and NaCl exhibited higher water uptake than NaCl-TiO_2. At 45°C, an interesting phenomenon occurs. At relative pressure between 0.75 and 0.9, all isotherms overlap; however, above 0.9 relative pressure NaCl-TiO_2 registered the highest water uptake which was above 45000 mg g^{-1} with a clear tendency of increased water uptake with temperature. These results suggest that NaCl-TiO_2 may also be attractive for applications requiring high temperature and high relative pressure. Moreover, although the water uptake of NaCl-SiO_2 has decreased at high temperature, it still reached 30000 mg· g^{-1}, this indicates that NaCl-SiO_2 could be a more suitable hygroscopic material at moderate temperature and high relative pressure, as it reaches its best performance at room temperature.

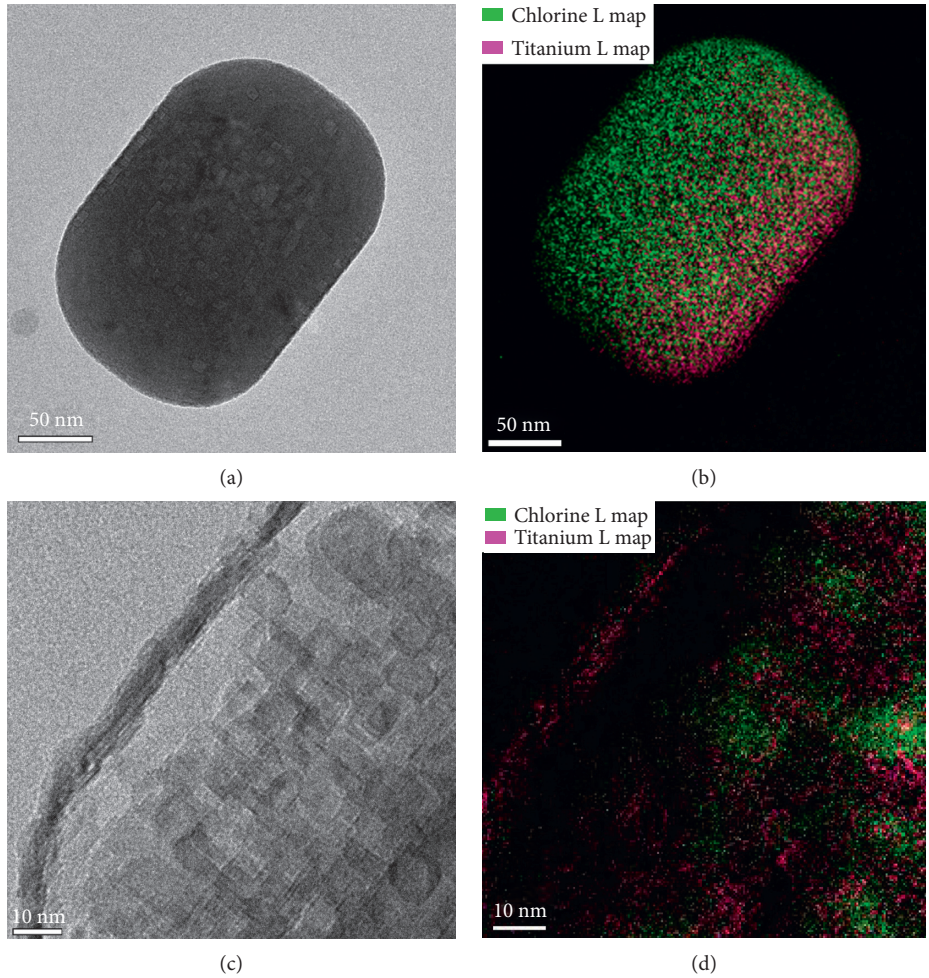

Figure 7: EFTEM-EELS high-resolution images of NaCl-TiO_2: (a, b) one particle of NaCl-TiO_2; (c, d) inset shows the detail of the thickness of TiO_2 surrounding the NaCl particle.

According to the hygroscopicity classification described by Callahan et al. [67] using the concept of equilibrium moisture content (EMC) introduced earlier by Scot et al. [68], the isotherms showed that NaCl-TiO_2 is a very good hygroscopic material, as the water uptake, i.e., equilibrium moisture content or EMC, occurs from very low relative humidity, even below 40% RH, as mentioned in the classification. Although NaCl and NaCl-SiO_2 showed lower water uptake at relative humidity below 70% RH, they are classified as very hygroscopic materials as well because the increase in the EMC is higher than 5% occurring below 60% RH. Another recent classification described by Murikipudi et al. [69] using a different method based on the sorption analysis lead to the same conclusions about these materials classifying them as very good hygroscopic materials.

Additionally, a per the adsorption isotherms at very low relative pressure, the specific surface area for each sample was determined (Table 1). NaCl-TiO_2 exhibited the highest specific surface area which is coherent with its adsorption capacity compared to the other samples. NaCl and NaCl-SiO_2 exhibited similar specific surface areas, which is also consistent with their respective adsorption capacity.

To study the kinetics of water adsorption, the water uptake as a function of time was recorded for each RH (Figure 12). Each point of the plots represents the time that a sample took to reach a maximum water uptake, i.e., water adsorption at equilibrium, at a fixed relative pressure.

The early stages of the water adsorption process are of a major interest because they allow identifying not only the ability of the material to adsorb high quantity of water molecules, but also indicate at which rate the adsorption has occurred. At all temperatures, NaCl-TiO_2 registered faster rate of adsorption and higher water uptake, especially for the first 60 minutes, which is critical for cloud seeding application. It is certain that once the clouds are seeded, rain is expected to fall within the first hour [70]. This interesting characteristic exhibited by NaCl-TiO_2 is attributed to the high energy interaction between the solid adsorbent and water vapor in the presence of TiO_2. For NaCl and NaCl-SiO_2, the kinetics of water adsorption is quite similar, and the adsorption rate is slower in comparison with NaCl-TiO_2. Moreover, the kinetics of adsorption indicates that it depends on temperature. In fact, the water uptake recorded for an equivalent time at equilibrium is higher at 45°C compared to the respective ones at 35°C and 25°C.

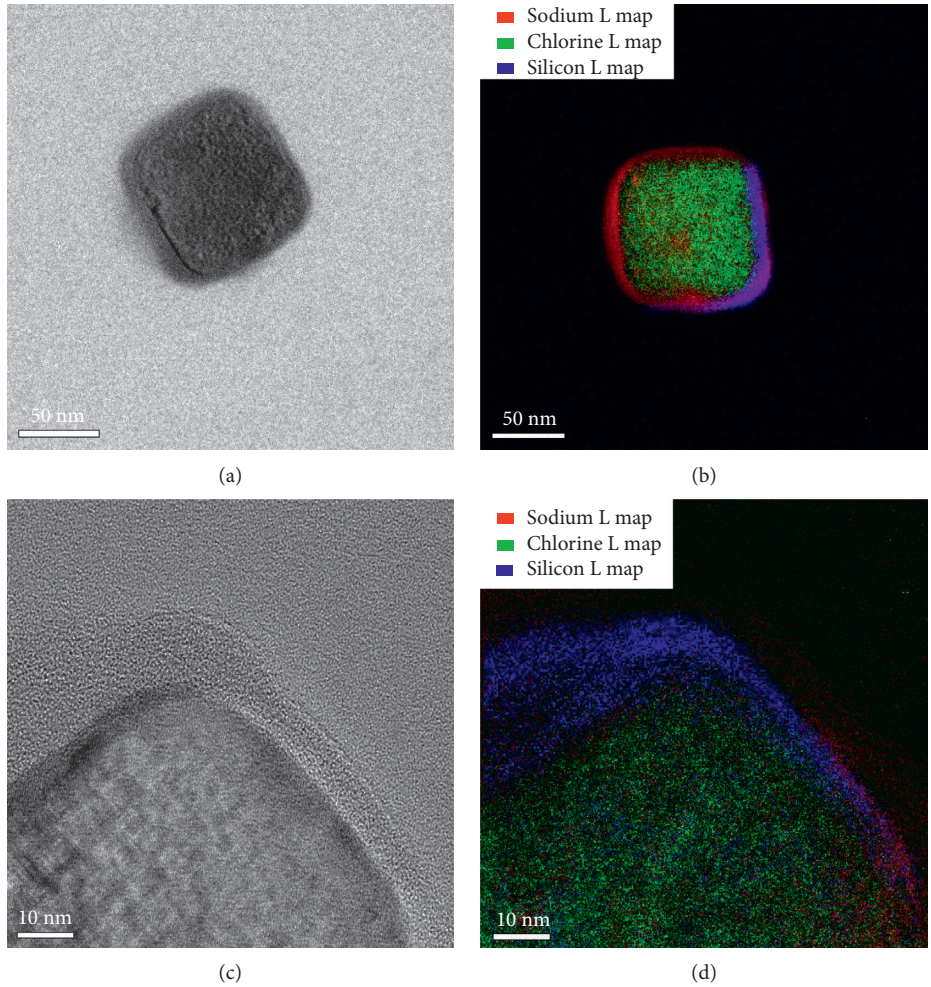

FIGURE 8: EFTEM-EELS high resolution images of NaCl-SiO_2: (a, b) one particle of NaCl-SiO_2; (c, d) inset shows the detail of the thickness of SiO_2 surrounding the NaCl particle.

In addition, using the adsorption isotherms at various temperatures, the isosteric heat of adsorption can be determined. The isosteric heat of adsorption, also called enthalpy of adsorption (ΔH_{ads}), indicates the strength of the interaction (bond) between the adsorbate (water molecules) and the solid adsorbent [71, 72]. This parameter represents the energy necessary for the heat of vaporization of moisture in a material during the adsorption process to exceed the latent heat of vaporization of pure water at a certain temperature [73]. It is derived from the Clausius–Clapeyron equation [48]:

$$\frac{\delta \ln P}{\delta (1/T)} = \frac{(\Delta H)}{R}, \quad (2)$$

where P is the absolute pressure, T is the temperature, ΔH is the enthalpy of adsorption, and R is the ideal gas constant.

The values of ΔH_{ads} were deduced from the data of pressure and temperature in equilibrium conditions represented by the three isotherms. The results are given as a slope $\Delta H_{ads}/R$ of the plot ln (P) versus (T^{-1}) (Figure 13).

ΔH_{ads} extracted from the plots of Figure 13 is shown in Figure 14. A particular variation of the NaCl-TiO_2 composite was observed. At the beginning of water adsorption, ΔH_{ads} is high around 45.2 kJ·mol^{-1}, and then it drops to 41.4 kJ·mol^{-1}, approximately.

This indicates that the high activity of polar sites on the surface of the solid adsorbent (i.e., high energy interaction) are covered with water molecules to form a monomolecular layer [74, 75], which is consistent with the previous results of the adsorption kinetics obtained for the first 60 minutes, and the significant water uptake at stage 1 (low relative pressure). Moreover, the low values of ΔH_{ads} are due to the progressive and slower filling of the less available sites, known to have lower bonding activation energies [76, 77]. Additionally, those initial values of ΔH_{ads} are higher than the latent heat of vaporization of pure water (43.1 kJ·mol^{-1} at 45°C). At these conditions, the energy of binding between the condensed water molecules and the adsorption sites of the solid adsorbent is higher than the energy of binding between the molecules of pure water that hold them together in the liquid phase, which is favorable for the adsorption process to occur [78, 79].

In the contrast, NaCl-SiO_2 showed high ΔH_{ads}, relatively constant throughout all the water adsorption stages. This can

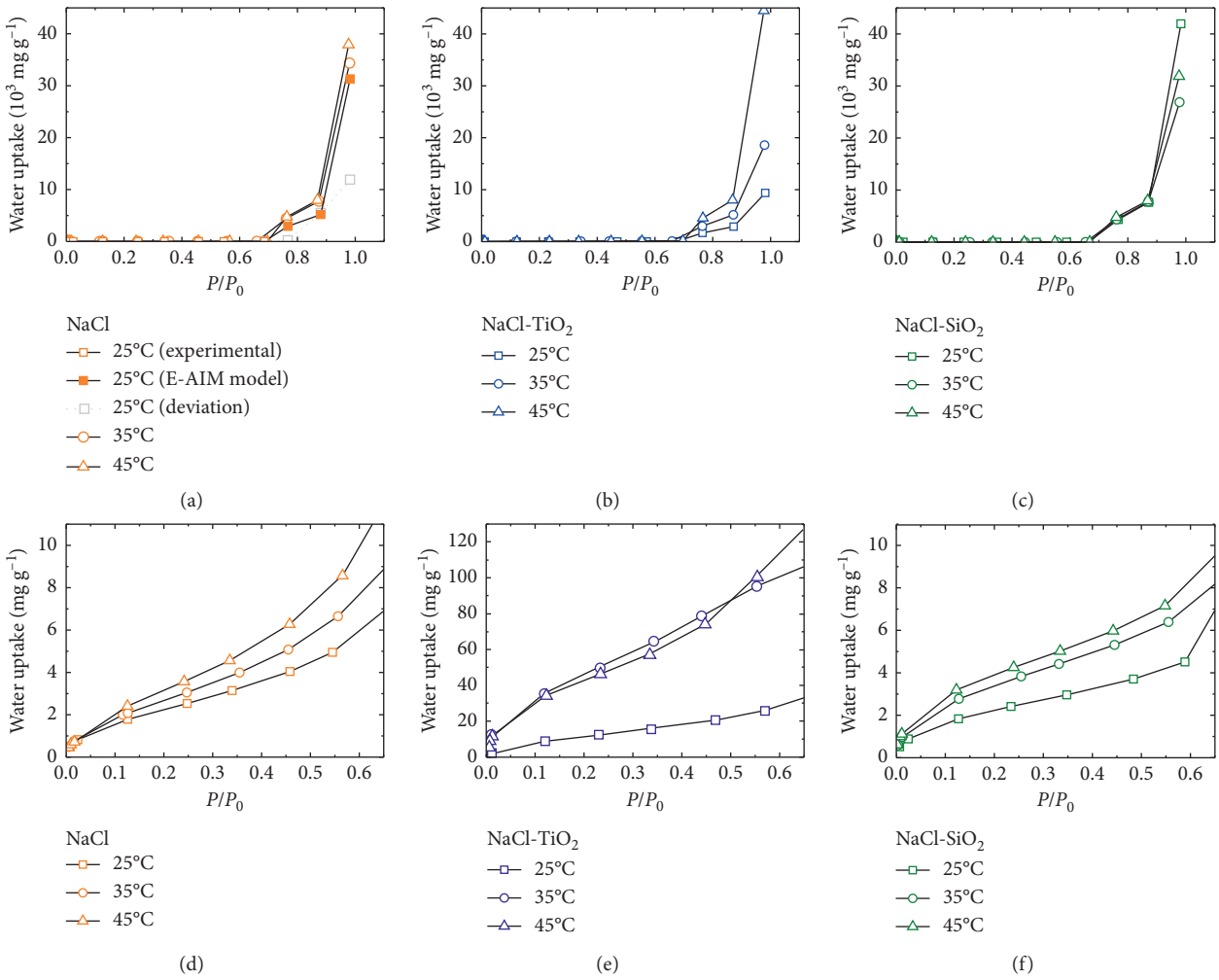

Figure 9: Water sorption analysis with isotherms at 25°C, 35°C, and 45°C: (a) and (d) for NaCl; (b) and (e) for NaCl-TiO_2; and (c) and (f) for NaCl-SiO_2, at relative pressure (0 to 1) top and an inset for low values of relative pressure (0 to 0.6) bottom. The isotherm of NaCl at 25°C shows a deviation obtained experimentally after the hygroscopic point and the correction as per the E-AIM model.

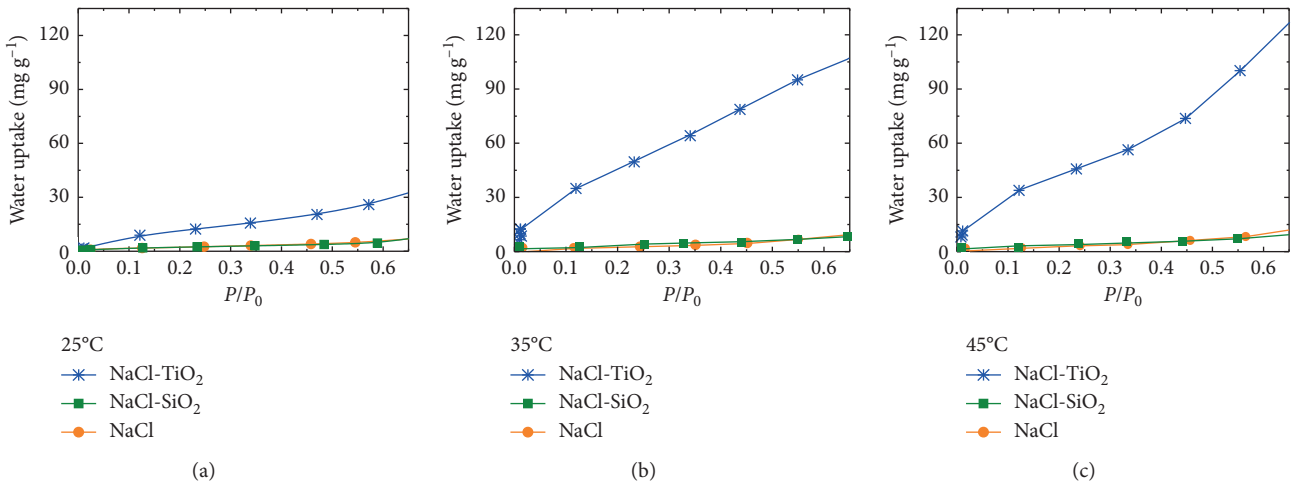

Figure 10: Comparison of isotherms of NaCl, NaCl-TiO_2, and NaCl-SiO_2, at low relative pressure from 0 to 0.7 at (a) 25°C, (b) 35°C, and (c) 45°C.

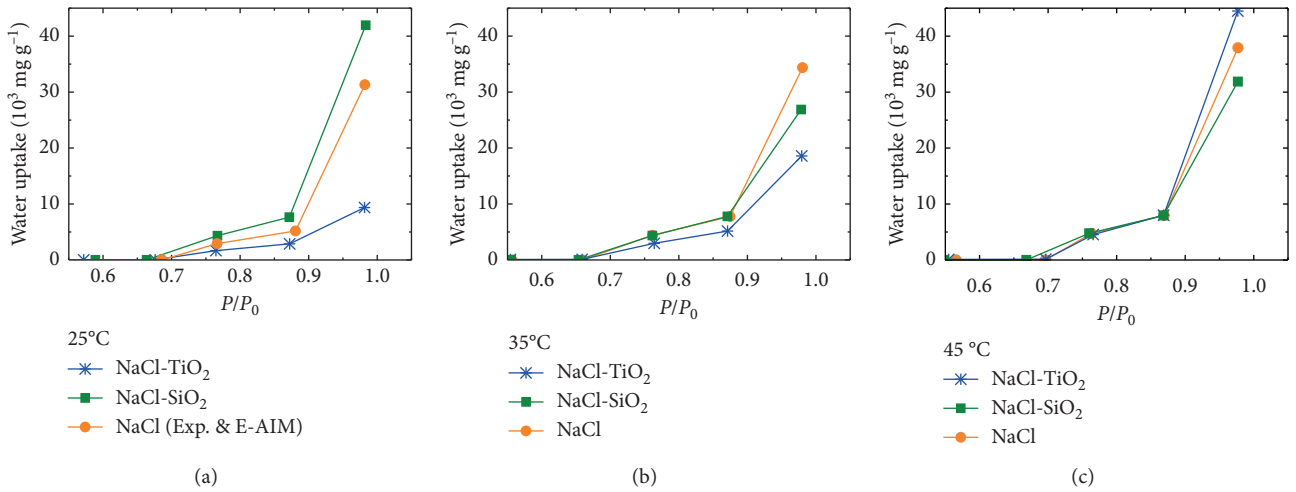

Figure 11: Comparison of isotherms of NaCl, NaCl-TiO_2, and NaCl-SiO_2, at high relative pressure from 0.7 to 1 at (a) 25°C, (b) 35°C, and (c) 45°C. The isotherm of NaCl at 25°C includes the experimental data and the correction as per the E-AIM model after the hygroscopic point as shown in Figure 9(a).

Table 1: Measured specific surface area of NaCl, NaCl-TiO_2, and NaCl-SiO_2 at 25°C, 35°C, and 45°C.

Material	Specific surface area[a] ($m^2 \cdot g^{-1}$)		
	25°C	35°C	45°C
NaCl	9.92	12.05	15.32
NaCl-TiO_2	49.14	201.86	175.30
NaCl-SiO_2	9.83	13.67	15.20

[a]Adsorbate: water vapor. $P/P_0 = 0.05$–0.35.

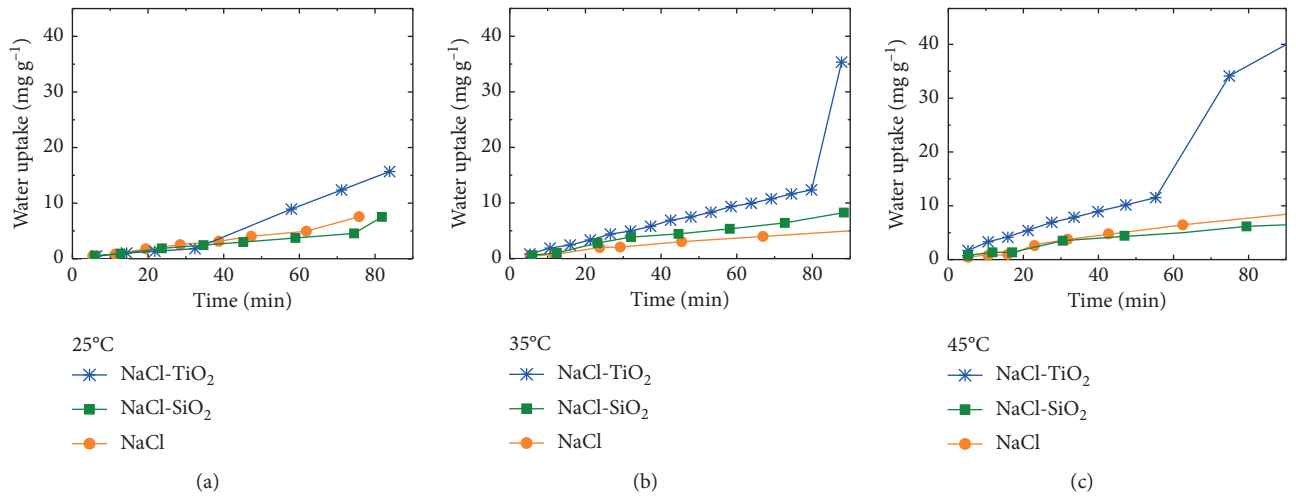

Figure 12: Kinetics of adsorption for NaCl, NaCl-TiO_2, and NaCl-SiO_2 at (a) 25°C, (b) 35°C, and (c) 45°C.

be considered as a valuable behavior in terms of adsorption process. However, NaCl has a slightly mixed trend of the isosteric heat of adsorption: at low water uptake, ΔH_{ads} is slightly above the latent heat of vaporization of pure water, but for high water uptake, up to 6000 mg·g^{-1} approximately, ΔH_{ads} decreases to lower values, and then again, ΔH_{ads} suddenly increases to 42 kJ·mol^{-1} during the last water uptake range. In addition, ΔH_{ads} for NaCl remains lower in all cases than the ones measured or NaCl-SiO_2. This suggests that NaCl-SiO_2 can be considered as a better adsorbent compared to NaCl.

3.3. Wettability Analysis. The water affinity of the samples was analyzed through *in situ* water condensation using ESEM (Figure 15).

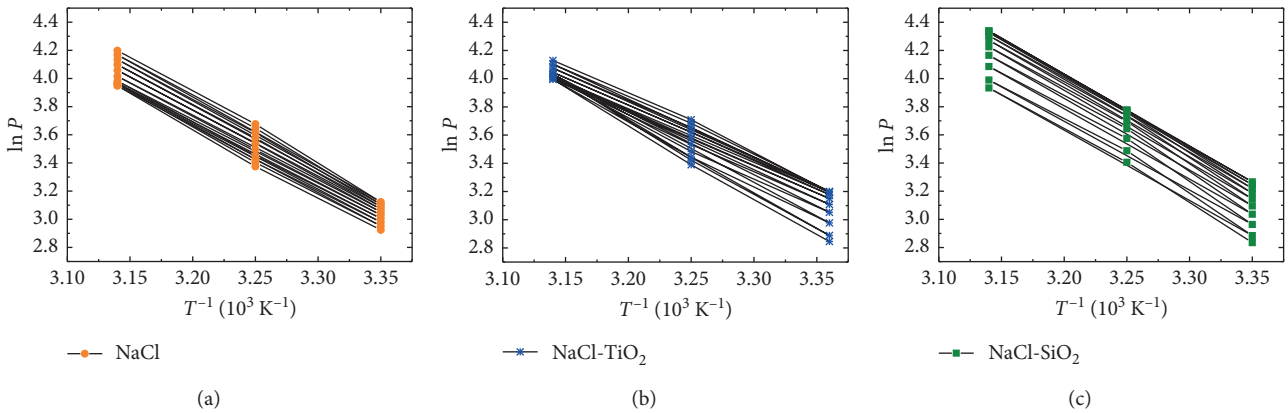

FIGURE 13: Variation of ln (P) vs. (T^{-1}) of (a) NaCl, (b) NaCl-TiO_2, and (c) NaCl-SiO_2.

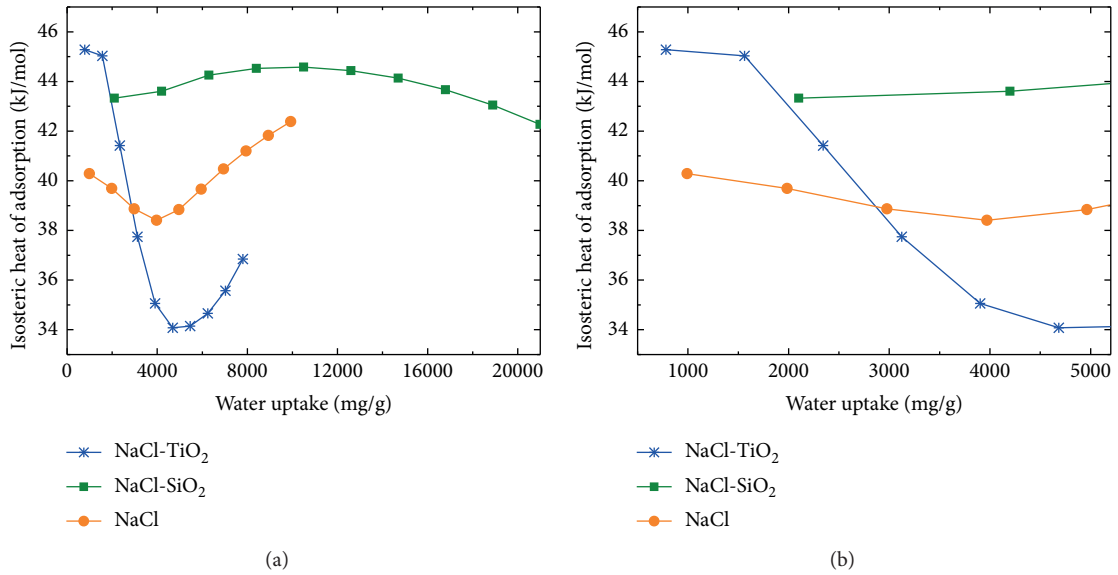

FIGURE 14: Isosteric heat of adsorption (ΔH_{ads}) of NaCl, NaCl-TiO_2, and NaCl-SiO_2: (a) full scale; (b) the inset shows the range 500–5000 mg·g^{-1}.

Since the surface wettability of these particles is the major interest to determine the extent of hydrophilicity and deliquescence, individual particles were analyzed. The pressure was increased gradually until the nucleation of the first water droplets was observed. At equilibrium, the water droplets stopped growing, while the pressure was still increasing, i.e., the water droplets reached their maximum diameter which represents the maximum water adsorption capacity. The diameter of the droplets was then measured and compared for the three types of samples. The final step consisted of reducing the pressure gradually until dried samples were observed, i.e., no more physical changes in the remaining particles. This last step clarified the understanding of the effect of the deliquescence process. Both NaCl-TiO_2 and NaCl-SiO_2 composites have developed larger water droplets compared to neat NaCl. D/D_0, which defines the ratio between the maximum diameter reached by the water droplet at equilibrium to the length of the solid particle, was determined to be ≈3.44, ≈3.76, and ≈2.26 for NaCl-TiO_2, NaCl-SiO_2, and NaCl, respectively. This indicates that both composite samples are more hydrophilic in nature than NaCl. It is noteworthy to emphasizing that the *in situ* condensation experiments at low temperature and pressure emulate the water vapor condensation process in the clouds with a close approximation, specifically, in warm clouds which are the main target for hygroscopic cloud seeding. Furthermore, once the condensation is achieved, the moisture was gradually removed until the particles are dried. The results showed that the size of neat NaCl remained relatively unchanged after the condensation experiments which suggests that both slow adsorption and a limited deliquescence process have occurred during the course of the experiment for neat NaCl. In contrast, after the condensation experiments, both composites NaCl-TiO_2 and NaCl-SiO_2 turned to a dispersed fine powder or they were entirely disintegrated which indicates a good deliquescence.

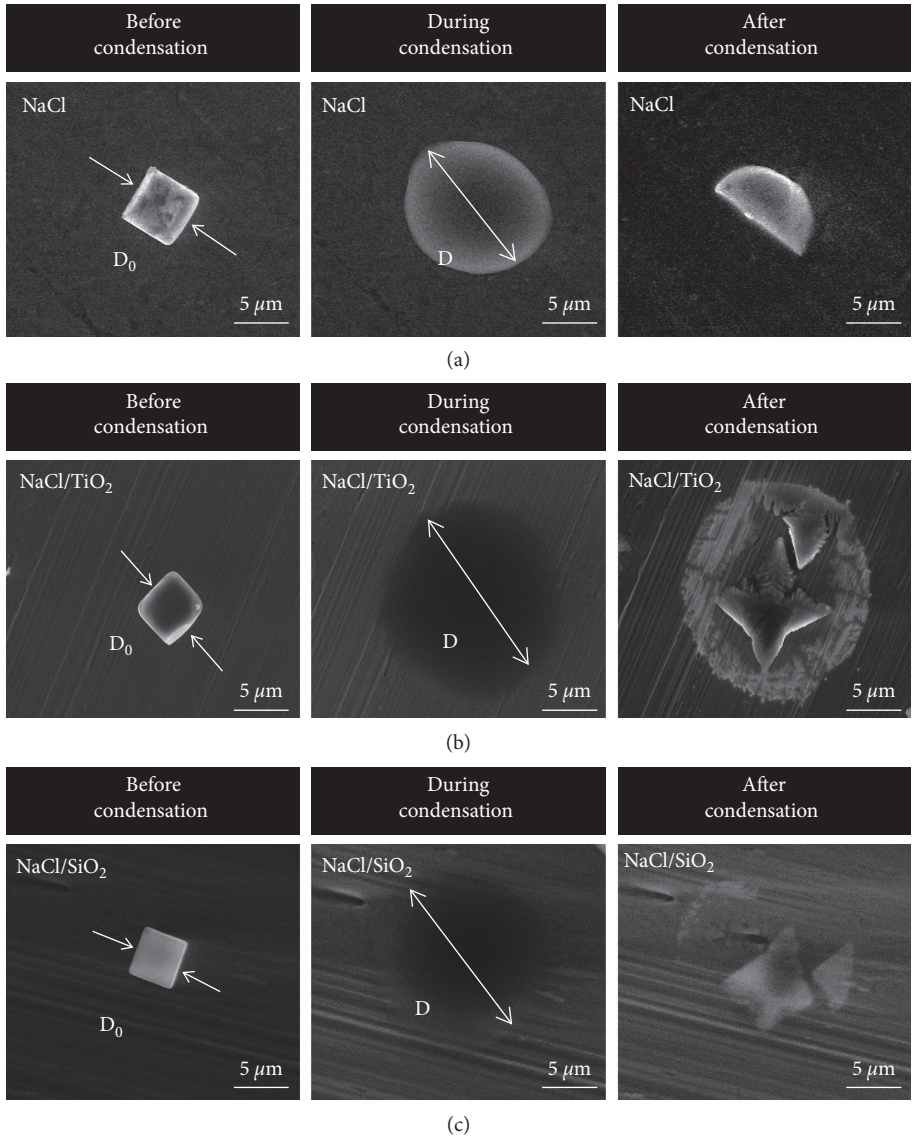

Figure 15: *In situ* condensation experiments inside ESEM at three key stages before condensation (left: dry samples); during condensation (center: samples at equilibrium), and after condensation (right: dried sample after water is removed) performed, respectively, on (a) NaCl (b) NaCl-TiO_2, and (c) NaCl-SiO_2.

Therefore, these results allowed to infer that both composites adsorb more water and deliquesce more effectively than neat NaCl.

3.4. Humidity-Controlled Dynamic Mechanical Analysis (DMA-RH). DMA-RH results are illustrated in Figure 16. Two stages can be identified: in stage 1, from 0 to 50–70% RH, the materials showed a distinctive water uptake related to an initial swelling and a subsequent softening of the area in contact with the DMA clamp. Thus, a negative displacement due to the penetration of the clamp inside the disc-shaped samples is recorded, while the moisture is increased in the chamber. In stage 2, from 50–70% RH to 90% RH, approximately, the materials experienced a steeper negative displacement since the clamp load has overcome the resilience of the materials which became softer due to the high amount of water adsorbed. At this stage, samples are deformed or dispersed. This behavior can be linked to the deliquescence process of the solid particles in water as seen in ESEM experiments and the isotherms.

NaCl presents no measurable water uptake at low relative humidity (stage 1). This is interpreted by a minor displacement as observed on the DMA-RH plot. At high RH (stage 2), a large displacement is recorded, and the deliquescence seemed to occur at 50–65% RH, where a sudden drop of the curve was observed. In contrast, the NaCl-TiO_2 composite started adsorbing water at the very beginning of RH (stage 1), and a significant displacement is recorded which stabilized and formed a plateau up to 60% RH, and then a rapid drop was observed in the range of 60–75% RH, at which the NaCl-TiO_2 composite deliquesces (stage 2). This indicates that

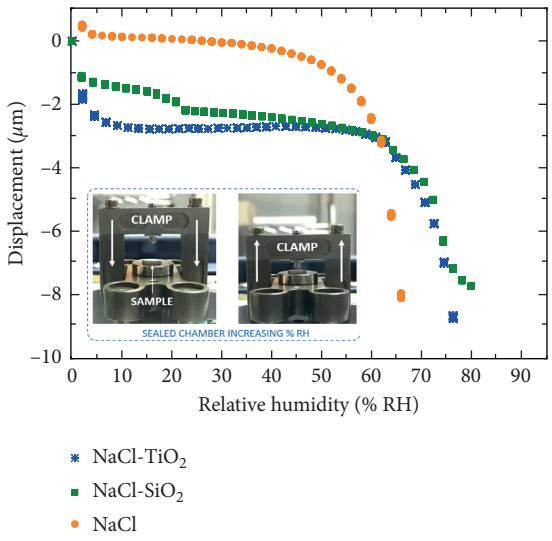

Figure 16: Humidity-controlled dynamic mechanical analysis of NaCl, NaCl-TiO_2, and NaCl-SiO_2.

NaCl-TiO_2 retained higher amount of moisture compared to NaCl. Moreover, NaCl-SiO_2 exhibited 3 stepwise water uptakes ranging from 0 to 20% RH as step 1, ranging from 20 to 60% RH as step 2, and starting above 60% RH as step 3 which suggests a multilayer adsorption. This indicates that NaCl-SiO_2 is behaving like NaCl-TiO_2 in terms of water uptake but at lower kinetics as NaCl-SiO_2 needs two stages of adsorption at low relative pressure to achieve similar water uptake than NaCl-TiO_2. Both water uptake curves showed that NaCl-SiO_2 deliquesces approximately at the same relative humidity as NaCl-TiO_2 (60 to 75% RH). Therefore, the two composites, NaCl-TiO_2 and NaCl-SiO_2, have demonstrated better water adsorption and deliquescence compared to NaCl but at higher rate for NaCl-TiO_2.

4. Conclusions

The successful optimization in terms of size and morphology of the commercial NaCl as per cloud seeding requirements allowed the development of the NaCl-TiO_2 and NaCl-SiO_2 composites. The effective coating process of NaCl preserved the cubic-shaped particles and size (0.5 to 6.9 μm) as per cloud seeding agent requirements.

Water adsorption analysis revealed that the NaCl-TiO_2 composite adsorbed high amount of water vapor at a faster rate in the cloud seeding conditions (low relative pressure) compared to NaCl and NaCl-SiO_2. In addition, NaCl-TiO_2 exhibited very promising adsorption properties for high-temperature applications as high as 45°C. Moreover, NaCl-SiO_2 was found to be potentially suitable hygroscopic material for high relative pressure applications while reaching its highest performance at room temperature.

In situ water condensation inside the ESEM and the DMA-RH tests confirmed that NaCl-TiO_2 composite possesses the best performances in terms of water adsorption capacity and deliquescence compared to NaCl. Likewise, NaCl-SiO_2 showed a comparable behavior as NaCl-TiO_2 but at lower kinetics.

Therefore, both composites NaCl-TiO_2 and NaCl-SiO_2 could be considered as promising hygroscopic materials and as potential candidates to replace the existing salt seeding agents for rain enhancement.

Data Availability

The (SEM and TEM images, the movies of the *in situ* ESEM, and the graphs) data used to support the findings of this study are available from the corresponding author upon request.

Conflicts of Interest

The authors declare that there are no conflicts of interest regarding the publication of this paper.

Acknowledgments

The financial support was provided by the National Center of Meteorology and Seismology, Abu Dhabi, UAE, under the UAE Research Program for Rain Enhancement.

Supplementary Materials

Water vapor adsorption kinetics of coated and uncoated NaCl: inset is an illustration of the adsorption among samples. (*Supplementary Materials*)

References

[1] J. U. Keller and R. Staudt, *Gas Adsorption Equilibria: Experimental Methods and Adsorptive Isotherms*, Springer Science & Business Media, Berlin, Germany, 2005.

[2] M. N. Golubovic, H. D. M. Hettiarachchi, and W. M. Worek, "Sorption properties for different types of molecular sieve and their influence on optimum dehumidification performance of desiccant wheels," *International Journal of Heat and Mass Transfer*, vol. 49, no. 17-18, pp. 2802–2809, 2006.

[3] X. Zheng, T. S. Ge, R. Z. Wang, and L. M. Hu, "Performance study of composite silica gels with different pore sizes and different impregnating hygroscopic salts," *Chemical Engineering Science*, vol. 120, pp. 1–9, 2014.

[4] S. Yildirim, B. Röcker, M. K. Pettersen et al., "Active packaging applications for food," *Comprehensive Reviews in Food Science and Food Safety*, vol. 17, no. 1, pp. 165–199, 2018.

[5] R. T. Bruintjes, "A review of cloud seeding experiments to enhance precipitation and some new prospects," *Bulletin of the American Meteorological Society*, vol. 80, no. 5, pp. 805–820, 1999.

[6] G. K. Mather, D. E. Terblanche, F. E. Steffens, and L. Fletcher, "Results of the South African cloud-seeding experiments using hygroscopic flares," *Journal of Applied Meteorology*, vol. 36, no. 11, pp. 1433–1447, 1997.

[7] Y. Tu, R. Wang, Y. Zhang, and J. Wang, "Progress and expectation of atmospheric water harvesting," *Joule*, vol. 2, no. 8, pp. 1452–1475, 2018.

[8] K. R. Spurny, "Atmospheric condensation nuclei P. J. Coulier 1875 and J. Aitken 1880 (historical review)," *Aerosol Science and Technology*, vol. 32, no. 3, pp. 243–248, 2000.

[9] D. M. Chate, P. S. P. Rao, M. S. Naik, G. A. Momin, P. D. Safai, and K. Ali, "Scavenging of aerosols and their chemical species by rain," *Atmospheric Environment*, vol. 37, no. 18, pp. 2477–2484, 2003.

[10] M. Ćurić and D. Janc, "Wet deposition of the seeding agent after weather modification activities," *Environmental Science and Pollution Research*, vol. 20, pp. 6344–6350, 2013.

[11] R. R. Czys and R. Bruintjes, "A review of hygroscopic seeding experiments to enhance rainfall," *The Journal of Weather Modification*, vol. 26, pp. 41–52, 1994.

[12] B. A. Silverman, "A critical assessment of hygroscopic seeding of convective clouds for rainfall enhancement," *Bulletin of the American Meteorological Society*, vol. 84, no. 9, pp. 1219–1230, 2003.

[13] R. T. Bruintjes, V. Salazar, T. A. Semeniuk, P. Buseck, D. W. Breed, and J. Gunkelman, "Evaluation of hygroscopic cloud seeding flares," *The Journal of Weather Modification*, vol. 44, pp. 69–94, 2012.

[14] H. Furukawa, F. Gándara, Y.-B. Zhang et al., "Water adsorption in porous metal-organic frameworks and related materials," *Journal of the American Chemical Society*, vol. 136, no. 11, pp. 4369–4381, 2014.

[15] H. Kim, S. Yang, S. R. Rao et al., "Water harvesting from air with metal-organic frameworks powered by natural sunlight," *Science*, vol. 356, no. 6336, pp. 430–434, 2017.

[16] H. X. Zhu, X. D. Li, and R. J. Yang, "A novel catalyst of warm-cloud seeding to enhance precipitation," *IOP Conference Series: Materials Science and Engineering*, vol. 137, Article ID 012002, 2016.

[17] J. G. Ji, R. Z. Wang, and L. X. Li, "New composite adsorbent for solar-driven fresh water production from the atmosphere," *Desalination*, vol. 212, no. 1-3, pp. 176–182, 2007.

[18] D. Kumar, K. Schumacher, C. du Fresne von Hohenesche, M. Grün, and K. K. Unger, "MCM-41, MCM-48 and related mesoporous adsorbents: their synthesis and characterisation," *Colloids and Surfaces A: Physicochemical and Engineering Aspects*, vol. 187-188, pp. 109–116, 2001.

[19] Y. Segal, A. Khain, M. Pinsky, and D. Rosenfeld, "Effects of hygroscopic seeding on raindrop formation as seen from simulations using a 2000-bin spectral cloud parcel model," *Atmospheric Research*, vol. 71, no. 1-2, pp. 3–34, 2004.

[20] D. Caro, W. Wobrock, and A. I. Flossmann, "A numerical study on the impact of hygroscopic seeding on the development of cloud particle spectra," *Journal of Applied Meteorology*, vol. 41, no. 3, pp. 333–350, 2002.

[21] W. A. Cooper, R. T. Bruintjes, and G. K. Mather, "Calculations pertaining to hygroscopic seeding with flares," *Journal of Applied Meteorology*, vol. 36, no. 11, pp. 1449–1469, 1997.

[22] N. Kuba and M. Murakami, "Effect of hygroscopic seeding on warm rain clouds - numerical study using a hybrid cloud microphysical model," *Atmospheric Chemistry and Physics*, vol. 10, no. 7, pp. 3335–3351, 2010.

[23] D. Rosenfeld and G. Gutman, "Retrieving microphysical properties near the tops of potential rain clouds by multispectral analysis of AVHRR data," *Atmospheric Research*, vol. 34, no. 1–4, pp. 259–283, 1994.

[24] C. G. Keyes Jr., G. W. Bomar, T. P. DeFelice, D. A. Griffith, and D. W. Langerud, *Guidelines for Cloud Seeding to Augment Precipitation*, American Society of Civil Engineers, Reston, VA, USA, 2016.

[25] D. K. Farmer, C. D. Cappa, and S. M. Kreidenweis, "Atmospheric processes and their controlling influence on cloud condensation nuclei activity," *Chemical Reviews*, vol. 115, no. 10, pp. 4199–4217, 2015.

[26] J. Rouquerol, F. Rouquerol, P. Llewellyn, G. Maurin, and K. S. Sing, *Adsorption by Powders and Porous Solids: Principles, Methodology and Applications*, Academic Press, Cambridge, MA, USA, 2nd edition, 2013.

[27] V. Bolis, C. Busco, M. Ciarletta et al., "Hydrophilic/hydrophobic features of TiO_2 nanoparticles as a function of crystal phase, surface area and coating, in relation to their potential toxicity in peripheral nervous system," *Journal of Colloid and Interface Science*, vol. 369, no. 1, pp. 28–39, 2012.

[28] H. Cheng and A. Selloni, "Hydroxide ions at the water/anatase TiO_2(101) interface: structure and electronic states from first principles molecular dynamics," *Langmuir*, vol. 26, no. 13, pp. 11518–11525, 2010.

[29] U. Aschauer, Y. He, H. Cheng, S.-C. Li, U. Diebold, and A. Selloni, "Influence of subsurface defects on the surface reactivity of TiO_2: water on anatase (101)," *The Journal of Physical Chemistry C*, vol. 114, no. 2, pp. 1278–1284, 2010.

[30] J. Goniakowski and M. J. Gillan, "The adsorption of H2O on TiO_2 and SnO_2(110) studied by first-principles calculations," *Surface Science*, vol. 350, no. 1-3, pp. 145–158, 1996.

[31] Ž. Knez and Z. Novak, "Adsorption of water vapor on silica, alumina, and their mixed oxide aerogels," *Journal of Chemical & Engineering Data*, vol. 46, no. 4, pp. 858–860, 2001.

[32] G. B. Alexader, "The effect of particle size on the solubility of amorphous silica in water," *The Journal of Physical Chemistry*, vol. 61, no. 11, pp. 1563-1564, 1957.

[33] G. B. Alexander, W. M. Heston, and R. K. Iler, "The solubility of amorphous silica in water," *The Journal of Physical Chemistry*, vol. 58, no. 6, pp. 453–455, 1954.

[34] V. Lenher and H. B. Merrill, "The solubility of silica," *Journal of the American Chemical Society*, vol. 39, no. 12, pp. 2630–2638, 1917.

[35] G. Okamoto, T. Okura, and K. Goto, "Properties of silica in water," *Geochimica et Cosmochimica Acta*, vol. 12, no. 1-2, pp. 123–132, 1957.

[36] J. D. Rimstidt and H. L. Barnes, "The kinetics of silica-water reactions," *Geochimica et Cosmochimica Acta*, vol. 44, no. 11, pp. 1683–1699, 1980.

[37] A. G. Tereshchenko, "Deliquescence: hygroscopicity of water-soluble crystalline solids," *Journal of Pharmaceutical Sciences*, vol. 104, no. 11, pp. 3639–3652, 2015.

[38] K. Hämeri, M. Väkevä, H.-C. Hansson, and A. Laaksonen, "Hygroscopic growth of ultrafine ammonium sulphate aerosol measured using an ultrafine tandem differential mobility analyzer," *Journal of Geophysical Research: Atmospheres*, vol. 105, no. D17, pp. 22231–22242, 2000.

[39] D. J. Cziczo, J. B. Nowak, J. H. Hu, and J. P. D. Abbatt, "Infrared spectroscopy of model tropospheric aerosols as a function of relative humidity: observation of deliquescence and crystallization," *Journal of Geophysical Research: Atmospheres*, vol. 102, no. D15, pp. 18843–18850, 1997.

[40] C. N. Cruz and S. N. Pandis, "Deliquescence and hygroscopic growth of mixed Inorganic–Organic atmospheric aerosol," *Environmental Science & Technology*, vol. 34, no. 20, pp. 4313–4319, 2000.

[41] I. N. Tang, "Phase transformation and growth of aerosol particles composed of mixed salts," *Journal of Aerosol Science*, vol. 7, no. 5, pp. 361–371, 1976.

[42] D. S. Covert, R. J. Charlson, and N. C. Ahlquist, "A study of the relationship of chemical composition and humidity to light scattering by aerosols," *Journal of Applied Meteorology*, vol. 11, no. 6, pp. 968–976, 1972.

[43] Y. Tai, H. Liang, A. Zaki et al., "Core/shell microstructure induced synergistic effect for efficient water-droplet formation and cloud-seeding application," *ACS Nano*, vol. 11, no. 12, pp. 12318–12325, 2017.

[44] K. Marbou, A. Al Ghaferi, and M. Jouiad, "In-situ characterization of Wettability alteration in Hopg," *SOP Transactions on Nanotechnology*, vol. 2374, pp. 1–10, 2015.

[45] N. Miljkovic, R. Enright, and E. N. Wang, "Effect of droplet morphology on growth dynamics and heat transfer during condensation on superhydrophobic nanostructured surfaces," *ACS Nano*, vol. 6, no. 2, pp. 1776–1785, 2012.

[46] C. Aprile, L. Maretti, M. Alvaro, J. C. Scaiano, and H. Garcia, "Long-lived (minutes) photoinduced charge separation in a structured periodic mesoporous titania containing 2,4,6-triphenylpyrylium as guest," *Dalton Transactions*, no. 40, pp. 5465–5470, 2008.

[47] Y. L. Du, Y. Deng, and M. S. Zhang, "Variable-temperature Raman scattering study on anatase titanium dioxide nanocrystals," *Journal of Physics and Chemistry of Solids*, vol. 67, no. 11, pp. 2405–2408, 2006.

[48] D. D. Do, *Adsorption Analysis: Equilibria and Kinetics*, Imperial College Press, London, UK, 1st edition, 1998.

[49] S. L. Clegg, K. S. Pitzer, and P. Brimblecombe, "Thermodynamics of multicomponent, miscible, ionic solutions "extended AIM aerosol thermodynamics model"," *The Journal of Physical Chemistry A*, vol. 96, no. , pp. 9470–9479, 1992.

[50] A. S. Wexler and S. L. Clegg, "Atmospheric aerosol models for systems including the ions H+, NH_4^+, Na^+, SO_4^{2-}, NO_3^-, Cl^-, Br^-, and H_2O," *Journal of Geophysical Research*, vol. 107, no. D14, 2002.

[51] E. Friese and A. Ebel, "Temperature dependent thermodynamic model of the system H^+–NH_4^+–Na^+–SO_4^{2-}–NO_3^-–Cl^-–H_2O," *The Journal of Physical Chemistry A*, vol. 114, no. 43, pp. 11595–11631, 2010.

[52] S. Ghorai, B. Wang, A. Tivanski, and A. Laskin, "Hygroscopic properties of internally mixed particles composed of NaCl and water-soluble organic acids," *Environmental Science & Technology*, vol. 48, no. 4, pp. 2234–2241, 2014.

[53] Y. Liu, Z. Yang, Y. Desyaterik, P. L. Gassman, H. Wang, and A. Laskin, "Hygroscopic behavior of substrate-deposited particles studied by micro-FT-IR spectroscopy and complementary methods of particle analysis," *Analytical Chemistry*, vol. 80, no. 3, pp. 633–642, 2008.

[54] C. Peng, B. Jing, Y.-C. Guo, Y.-H. Zhang, and M.-F. Ge, "Hygroscopic behavior of multicomponent aerosols involving NaCl and dicarboxylic acids," *The Journal of Physical Chemistry A*, vol. 120, no. 7, pp. 1029–1038, 2016.

[55] F. D. Pope, B. J. Dennis-Smither, P. T. Griffiths, S. L. Clegg, and R. A. Cox, "Studies of single aerosol particles containing malonic acid, glutaric acid, and their mixtures with sodium chloride. I. Hygroscopic growth," *The Journal of Physical Chemistry A*, vol. 114, no. 16, pp. 5335–5341, 2010.

[56] C. B. Richardson and T. D. Snyder, "A study of heterogeneous nucleation in aqueous solutions," *Langmuir*, vol. 10, no. 7, pp. 2462–2465, 1994.

[57] C.-P. Lin, H. Chen, A. Nakaruk, P. Koshy, and C. C. Sorrell, "Effect of annealing temperature on the photocatalytic activity of TiO_2 thin films," *Energy Procedia*, vol. 34, pp. 627–636, 2013.

[58] Q. Ma, H. He, and Y. Liu, "In situ DRIFTS study of hygroscopic behavior of mineral aerosol," *Journal of Environmental Sciences*, vol. 22, no. 4, pp. 555–560, 2010.

[59] Z. Mouline, K. Asai, Y. Daiko, S. Honda, S. Bernard, and Y. Iwamoto, "Amine-functionalized polycarbosilane hybrids for CO2-selective membranes," *Journal of the European Ceramic Society*, vol. 37, no. 16, pp. 5213–5221, 2017.

[60] G. E. Ewing and S. J. Peters, "Adsorption of water on NaCl," *Surface Review and Letters*, vol. 04, no. 04, pp. 757–770, 1997.

[61] B. Wassermann, S. Mirbt, J. Reif, J. C. Zink, and E. Matthias, "Clustered water adsorption on the NaCl (100) surface," *The Journal of Chemical Physics*, vol. 98, no. 12, pp. 10049–10060, 1993.

[62] D. D. Weis and G. E. Ewing, "Water content and morphology of sodium chloride aerosol particles," *Journal of Geophysical Research: Atmospheres*, vol. 104, no. D17, pp. 21275–21285, 1999.

[63] C. J. Walcek, "Cloud cover and its relationship to relative humidity during a springtime midlatitude cyclone," *Monthly Weather Review*, vol. 122, no. 6, pp. 1021–1035, 1994.

[64] R. T. Wetherald and S. Manabe, "An investigation of cloud cover change in response to thermal forcing," *Climatic Change*, vol. 8, no. 1, pp. 5–23, 1986.

[65] J. B. Condon, *Surface Area and Porosity Determinations by Physisorption: Measurements and Theory*, Elsevier, Amsterdam, Netherlands, 2006.

[66] K. S. W. Sing, "Reporting physisorption data for gas/solid systems with special reference to the determination of surface area and porosity (Provisional)," *Pure and Applied Chemistry*, vol. 54, no. 11, pp. 2201–2218, 1982.

[67] J. C. Callahan, G. W. Cleary, M. Elefant, G. Kaplan, T. Kensler, and R. A. Nash, "Equilibrium moisture content of pharmaceutical excipients," *Drug Development and Industrial Pharmacy*, vol. 8, no. 3, pp. 355–369, 1982.

[68] M. W. Scott, H. A. Lieberman, and F. S. Chow, "Pharmaceutical applications of the concept of equilibrium moisture contents," *Journal of Pharmaceutical Sciences*, vol. 52, no. 10, pp. 994–998, 1963.

[69] V. Murikipudi, P. Gupta, and V. Sihorkar, "Efficient throughput method for hygroscopicity classification of active and inactive pharmaceutical ingredients by water vapor sorption analysis," *Pharmaceutical Development and Technology*, vol. 18, no. 2, pp. 348–358, 2013.

[70] S. Patil, "A study of artificial rainfall," *International Journal of Multifaceted and Multilingual Studies*, vol. 3, 2016.

[71] E. Shotton and N. Harb, "The effect of humidity and temperature on the equilibrium moisture content of powders," *Journal of Pharmacy and Pharmacology*, vol. 17, no. 8, pp. 504–508, 1965.

[72] S. Builes, S. I. Sandler, and R. Xiong, "Isosteric heats of gas and liquid adsorption," *Langmuir*, vol. 29, no. 33, pp. 10416–10422, 2013.

[73] N. A. Aviara, O. O. Ajibola, and U. O. Dairo, "PH-postharvest technology," *Biosystems Engineering*, vol. 83, no. 4, pp. 423–431, 2002.

[74] A. H. Al-Muhtaseb, W. A. M. McMinn, and T. R. A. Magee, "Water sorption isotherms of starch powders," *Journal of Food Engineering*, vol. 61, no. 3, pp. 297–307, 2004.

[75] A. H. Al-Muhtaseb, W. A. M. McMinn, and T. R. A. Magee, "Water sorption isotherms of starch powders. Part 2: thermodynamic characteristics," *Journal of Food Engineering*, vol. 62, no. 2, pp. 135–142, 2004.

[76] S. Sircar, R. Mohr, C. Ristic, and M. B. Rao, "Isosteric heat of adsorption: theory and experiment," *The Journal of Physical Chemistry B*, vol. 103, no. 31, pp. 6539–6546, 1999.

[77] M. Yazdani, P. Sazandehchi, M. Azizi, and P. Ghobadi, "Moisture sorption isotherms and isosteric heat for pistachio," *European Food Research and Technology*, vol. 223, no. 5, pp. 577–584, 2006.

[78] M. Masuzawa and C. Sterling, "Gel-water relationships in hydrophilic polymers: thermodynamics of sorption of water vapor," *Journal of Applied Polymer Science*, vol. 12, no. 9, pp. 2023–2032, 1968.

[79] E. Tsami, "Net isosteric heat of sorption in dried fruits," *Journal of Food Engineering*, vol. 14, no. 4, pp. 327–335, 1991.